



Measurement of b hadron Lifetimes in the modes
 $B^+ \rightarrow J/\psi K^+$, $B^0 \rightarrow J/\psi K^{*0}$, $B^0 \rightarrow J/\psi K_s^0$, and $\Lambda_b^0 \rightarrow J/\psi \Lambda^0$, and measurement of the
 B^+/B^0 and Λ_b^0/B^0 lifetime ratios.

Text for the blessed web page – CDF note 10071

The CDF Collaboration
URL <http://www-cdf.fnal.gov>
(Dated: February 23, 2010)

In this note, we present an updated measurement of the b -hadron lifetimes in the modes $B^+ \rightarrow J/\psi K^+$, $B^0 \rightarrow J/\psi K^{*0}$, $B^0 \rightarrow J/\psi K_s^0$ and $\Lambda_b^0 \rightarrow J/\psi \Lambda^0$, based upon 4.3 fb^{-1} of luminosity collected between February 2002 and January 2009. We measure

$$\begin{aligned}c\tau(B^+) &= 491.4 \pm 2.6 \text{ (stat.)} \pm 2.6 \text{ (syst.) } \mu\text{m}, \\c\tau(B^0) &= 451.7 \pm 3.0 \text{ (stat.)} \pm 2.5 \text{ (syst.) } \mu\text{m}, \\c\tau(\Lambda_b^0) &= 460.8 \pm 13.4 \text{ (stat.)} \pm 4.1 \text{ (syst.) } \mu\text{m}.\end{aligned}$$

This corresponds to

$$\begin{aligned}\tau(B^+) &= 1.639 \pm 0.009 \text{ (stat.)} \pm 0.009 \text{ (syst.) ps}, \\ \tau(B^0) &= 1.507 \pm 0.010 \text{ (stat.)} \pm 0.008 \text{ (syst.) ps}, \\ \tau(\Lambda_b^0) &= 1.537 \pm 0.045 \text{ (stat.)} \pm 0.014 \text{ (syst.) ps}.\end{aligned}$$

We also present a measurement of the lifetime ratios

$$\begin{aligned}\tau(B^+)/\tau(B^0) &= 1.088 \pm 0.009 \text{ (stat.)} \pm 0.004 \text{ (syst.)}, \\ \tau(\Lambda_b^0)/\tau(B^0) &= 1.020 \pm 0.030 \text{ (stat.)} \pm 0.008 \text{ (syst.)}\end{aligned}$$

I. INTRODUCTION

The lifetime of ground state hadrons containing a b quark and lighter quarks is largely determined by the charged weak decay of the b quark. The spectator model (Fig. 1), which ignores the other quarks in the hadron, predicts equal lifetimes for B^0 , B^+ , and Λ_b^0 hadrons. In reality, several effects change these lifetimes by up to about 10%. They include kinematic effects and interactions between the spins of the b quark and the light quark cloud, as well as spectator effects known as Pauli Interference (Fig. 2), weak scattering, and weak annihilation (Fig. 3). A theoretical approach to b hadron observables known as the heavy quark expansion (HQE) organizes these effects into an expansion in powers of Λ_{QCD}/m_b :

$$\Gamma = \frac{G_F^2 m_b^5}{192\pi^3} |V_{cb}|^2 \cdot \left[A_0 + A_2 \left(\frac{\Lambda_{QCD}}{m_b} \right)^2 + A_3 \left(\frac{\Lambda_{QCD}}{m_b} \right)^3 \right]. \quad (1)$$

In this expansion, kinematic effects enter at second order, while the spectator effects illustrated in Fig. 2 and Fig. 3 enter at third order.

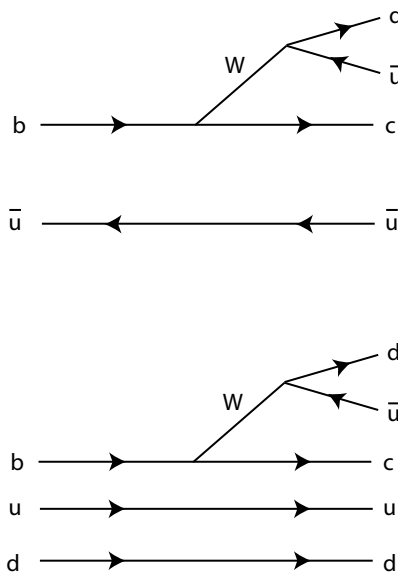


FIG. 1: Spectator diagrams in b hadron decay. Top: b meson decay. Bottom: b baryon decay.

The lifetime ratio $\tau(B^+)/\tau(B^0)$ is predicted[1][2][3][4] to be in the range 1.04-1.08. For the $\tau(\Lambda_b^0)/\tau(B^0)$ one encounters a much wider range, from 0.83-0.93, indicating a lack of agreement among theoretical predictions[5]. Experimentally, the measured Λ_b^0 lifetime has historically been at the lower end of the theoretical range. CDF has recently produced two high-precision measurements of the Λ_b^0 lifetime, one using fully reconstructed $J/\psi\Lambda^0$ events collected with a dimuon trigger[6] and a second using fully reconstructed hadronic decays of Λ_b^0 collected with high precision displaced track trigger[7]. Both of these recent measurements have fallen significantly above the world average.

The world average B^+ and B^0 lifetimes are dominated by a single experiment, Belle, whose published result [8] is a combination of many channels including fully reconstructed channels with a J/ψ or with other hadrons, and semileptonic channels. Those measurements are now limited by systematic uncertainties.

This analysis is a precise measurement of B^+ , B^0 , and Λ_b^0 lifetimes. It updates our previous Λ_b^0 lifetime measurement ([6]) with 4.3 fb^{-1} of data, and in addition now provides the world's best measurement of the B^+ and B^0 lifetimes, as well as their ratio. The measurements are performed using b -hadron decays to states containing a J/ψ . Statistical uncertainties on the B^+ and B^0 lifetimes are now at the level of about $3 \mu\text{m}$. We therefore aim to control tightly the systematic uncertainties for those channels. The same techniques are then used in the measurement of the Λ_b^0 lifetime.

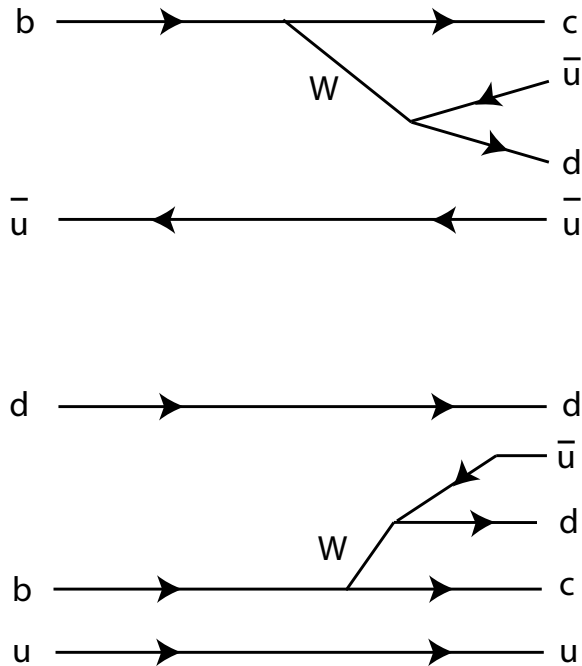


FIG. 2: The lifetime is defined by all possible decays. The above diagrams show typical Pauli interference (PI) diagrams in b hadron decay which make different contributions to the hadron lifetimes. Top: b meson decay. Bottom: b baryon decay. In general, Pauli interference includes all short-distance interactions. The diagrams demonstrate typical contributions mediated by a charged weak boson. Pauli interference in the B^+ meson prolongs the lifetime relative to that of the B^0 , and increases the lifetime of the Λ_b^0 by about 3% with respect to the B^0 .

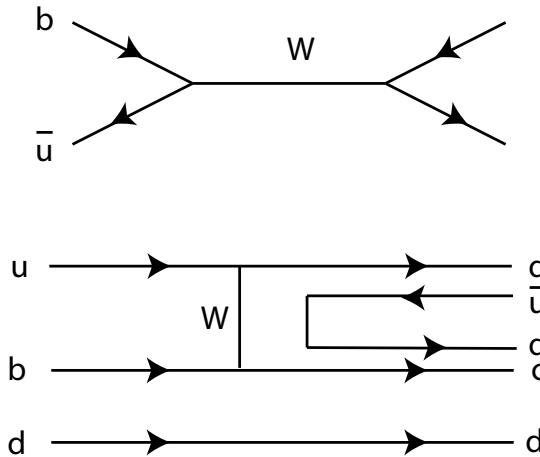


FIG. 3: Typical weak annihilation (WA) diagrams in b meson decay (top) and weak scattering diagrams in baryon decay (bottom). As in the case of PI diagrams, these are merely examples of a whole class of short distance interactions. These diagrams do not contribute much to meson lifetimes, but do decrease that of the Λ_b^0 by about 7%.

II. ANALYSIS STRATEGY AND TECHNIQUES

The goal of this set of measurements is to measure lifetimes as precisely as possible and in a consistent way across all of channels considered. We control systematic uncertainties to the level necessitated by the B^0 and B^+ modes, and then apply the same methods to the Λ_b^0 . We use the vertex formed by the two tracks from the J/ψ as an estimate of the transverse decay length (defined below) so that systematic uncertainties common to the estimate of decay length cancel to some extent in the ratio of lifetimes.

In this note we use t to denote the reconstructed proper decay time of a single b hadron and τ to denote the mean life of a species of b hadron. The proper decay length (PDL) of a b hadron is the difference (in ct , where c is the speed of light) between production and decay in the Lorentz frame of the hadron. Analysis objects used to estimate this quantity are: tracks (to estimate the b hadron four momentum and the decay point, or secondary vertex) and the beamline (to estimate the production point, or primary vertex). The transverse decay length L_{xy} of a single decay is defined as

$$L_{xy} = \frac{\mathbf{V} \cdot \vec{p}_T}{|\vec{p}_T|}, \quad (2)$$

where \mathbf{V} is the vector pointing from the primary to the secondary vertex position and \vec{p}_T is the transverse momentum. Both \mathbf{V} and \vec{p}_T are two dimensional vectors, defined in the $r\phi$ plane. The proper decay length ct is computed as:

$$ct = \frac{ML_{xy}}{p_T}. \quad (3)$$

A. Track reconstruction and relevant detector and trigger description

The data used in this analysis are selected from the J/ψ dataset, collected by CDF from March 2002 to January 2009. It corresponds to an integrated luminosity of 4.3 fb^{-1} .

Tracks in CDF are reconstructed using a cylindrical drift chamber, the Central Outer Tracker (COT), immersed in a 1.4 T axial magnetic field, providing up to 96 single position measurements at radii between 40 and 137 cm. The concentric layers of wires in the COT are segmented radially into eight ‘‘superlayers’’. Axial superlayers 1, 3, 5, and 7 have wires running parallel to the \hat{z} direction and stereo superlayers 2, 4, 6, and 8 have wires making an angle of $\pm 2^\circ$ with respect to \hat{z} (CDF uses a coordinate system in which the \hat{z} axis points parallel to the beam in the direction taken by the protons, while the \hat{x} axis points outward from the accelerator ring, and the \hat{y} axis points upwards). Tracks having $|\eta| < 1$, where $\eta = -\ln(\tan(\theta/2))$, θ being the polar angle of the track in the CDF coordinate system, are accepted by the COT, and their p_T is measured with a resolution of $\sigma(p_T)/p_T \approx 0.15\% p_T/(\text{GeV}/c)$. Precision impact parameter information comes from the Silicon Vertex Detector (SVX), which provides five position measurements in both $r\phi$ and z from 2.5 to 10.6 cm, and from the intermediate silicon layers (ISL), which provides additional measurements between the SVX and the ISL. J/ψ candidates are selected using muon systems called the Central Muon Detector (CMU), which covers the region $|\eta| < 0.6$, the Central Muon Extension (CMX) which covers the region from $0.6 < |\eta| < 1.0$, and the Central Muon Upgrade (CMP) which covers approximately the same pseudorapidity region as the CMU, but which lies behind an additional 60 cm of steel. Hadronic and electromagnetic calorimetry is not important to this analysis, and will not be described here.

Events containing a J/ψ are first selected with a dimuon trigger which uses information from the COT and the muon systems. The trigger selection begins with the eXtremely Fast Tracker (XFT, a trigger processor) which uses a coarsely binned drift time in the COT to find tracks and measure their p_T with a resolution of $\sigma(p_T)/p_T \approx 2.0\% p_T/(\text{GeV}/c)$ for the Level 1 decision. A second trigger processor, the XTRP, extrapolates these tracks to the muon systems and attempts to associate muon hits to the track. For the J/ψ dataset, we require two XFT tracks of opposite charge, and two muon hit clusters (stubs) from either the CMU or the CMX system on each track. The matching requirements in track-stub displacement and angular displacement are adjusted to be efficient for low- p_T muons which undergo multiple-scattering in the calorimeters. Tracks in the CMU system are required to have $p_T > 1.5 \text{ GeV}/c$, while those CMX system are required to have $p_T > 2.0 \text{ GeV}/c$. Opposite-charge and opening-angle cuts are imposed at Level 2. At Level 3, a full event reconstruction is performed, and a cut on invariant mass of the two muons between 2.7 and $4.0 \text{ GeV}/c^2$ is imposed. The two muon tracks are required to have $\Delta z < 5 \text{ cm}$ at the point of closest approach to the origin.

Tracks in CDF are reconstructed using a Kalman filtering algorithm that propagates both hit and alignment information into reconstructed track parameters and their errors; information on energy loss and multiple coulomb scattering upstream of the COT is properly accounted for in this propagation. The particle mass appropriate to the particle hypothesis (muon, pion, proton, kaon) is used to compute multiple scattering and energy loss. For daughter tracks from K_s^0 and Λ^0 only material outside of their decay radius is considered in the track fit. Any hits present on a K_s^0 or (Λ^0) daughter track closer to the beamspot than the decay radius is dropped from the final track fit. Because daughter tracks which have incorrect SVX II hits attached may bias the vertex constrained fit for the K_s^0 (Λ^0), we use COT-only tracks to compute the radius at the intersection point.

The transverse profile of the luminous region inside the CDF detector can be described by Gaussian functions in x and y . The means of those Gaussians define the beam position. Their width (approximately 30 μm) varies along the length of the interaction region due to the focusing of the beams. In CDF, the beam position is measured using the silicon tracking detectors as well as the COT. It is calculated and stored on a run by run basis.

B. Further selection requirements

Further requirements on selected events are imposed in order to reduce the background. To separate muons from a background of hadron punch-through and decay-in-flight, the χ^2 of the position match between track segments in the CMU and CMX and the extrapolated track is required to be less than 9 in the $r\phi$ plane offline, and we require that $p_T > 1.5$ GeV/c. Since the analysis requires precise vertex information, we select only muons whose corresponding tracks have 3 or more $r - \phi$ hits in the SVX II. There is no additional requirement on the number of COT hits per segment. The two muons are fit to a common vertex using a kinematic fitter, which returns a χ^2 as well as an estimated vertex position, and refitted, or vertex-constrained tracks. The refitted tracks are used to estimate derived quantities like p_T and reconstructed dimuon mass. We require that $\text{prob}(\chi^2) > 0.001$, and that the fitted mass be in the range $3.014 < m(\mu\mu) < 3.174$ GeV/c². The transverse decay distance to the primary vertex, L_{xy} , and its error, σ_{xy} , are also obtained and are used after all cuts are made to estimate the proper decay time.

To reconstruct K^{*0} , K_s^0 and Λ^0 in J/ψ events, we fit pairs of oppositely charged tracks to a common vertex. Both tracks must have at least 5 COT hits in at least 2 axial and 2 stereo superlayers. The daughter tracks should not be identified as the muon tracks. For K_s^0 , both tracks are given the pion mass hypothesis. For Λ^0 , since one of the daughter tracks should be a proton and the other a pion, we make both hypotheses and accept the one with the mass closest to the PDG value. For K^{*0} one the daughter tracks should be a kaon and the other a pion, we make both assumptions and accept the one with the mass closest to the PDG value. This procedure incurs a small systematic uncertainty, discussed in section IV.

For each selected track pair, we obtain its vertex position and vertex constrained invariant mass. K_s^0 and Λ^0 candidates whose transverse decay length (with respect to the J/ψ vertex) are below 0.1 cm are removed; the decay length significance is required to be greater than 6 for the K_s^0 and 4 for the Λ^0 . After the vertex fit, the fitted mass is then required to be in a mass window; for the K^{*0} this window is $0.84 < m(K\pi) < 0.96$ GeV/c² (the lower range is selected in order to avoid reflections from the $\phi \rightarrow K^+K^-$), while for the K_s^0 it is $0.473 < m(\pi\pi) < 0.523$ GeV/c² and for the Λ^0 it is $1.107 < m(p\pi) < 1.125$ GeV/c². We use an active veto to remove cross-contamination between the K^0 and the Λ^0 . Thus, when we are reconstructing K_s^0 's (Λ^0 's), we also try the proton/pion (pion/pion) mass hypothesis for each track pair. If the mass falls in the range 1.1085 - 1.1235 GeV/c² (0.48175 - 0.51425 GeV/c²), we no longer consider this a K_s^0 (Λ^0) candidate.

Next, we reconstruct the modes $B^+ \rightarrow J/\psi K^+$, $B^0 \rightarrow J/\psi K^{*0}$, $B^0 \rightarrow J/\psi K_s^0$, and $\Lambda_b^0 \rightarrow J/\psi \Lambda^0$ by performing a kinematic fit of all b hadron daughter tracks to the appropriate topology (two spatially separated vertices in the case of $\Lambda_b^0 \rightarrow J/\psi \Lambda^0$ and $B^0 \rightarrow J/\psi K_s^0$, one vertex in all other cases). In this fit, a mass constraint is applied to the J/ψ and pointing constraints are applied to the K_s^0 and Λ^0 . Additional cuts requiring consistency with the fit assumptions (common vertex or vertices, mass and pointing constraints) are then applied.

The cuts on the transverse momenta of B^+ , B^0 , Λ_b^0 , K^+ , K_s^0 , K^{*0} , and Λ^0 , the invariant mass of K_s^0 , K^{*0} , and Λ^0 , the vertex probability of B^+ , B^0 's, Λ_b^0 and the L_{xy} significance (K_s^0 and Λ^0) were obtained via an optimization procedure which maximizes the quantity $S/\sqrt{S+B}$ over all of the cuts, where S is the number of signal events and B the number of background events. The signal events were produced with a full simulation which includes trigger emulation and a complete GEANT representation of CDF. The background events were taken from the sidebands of the data mass distribution. The sideband regions used in optimization are not part of the data used in the lifetime fit to avoid any potential bias. In $S/\sqrt{S+B}$, S is always multiplied by the ratio of signal events observed in the data to that in the Monte Carlo to properly weight the relative signal and background sample sizes in the optimization. For each mode, the maximum of $S/\sqrt{S+B}$ was found simultaneously with respect to all varying quantities. The cut values not listed above are summarized in the following list:

- $B^+ \rightarrow J/\psi K^+$
 - $p_T(K^+) > 2.0 \text{ GeV}/c$
 - $p_T(B^+) > 6.2 \text{ GeV}/c$
 - $\text{prob}(\chi^2)[B^+] > 0.001$
- $B^0 \rightarrow J/\psi K^{*0}$
 - $p_T(K^{*0}) > 3.0 \text{ GeV}/c$
 - $p_T(B^0) > 6.4 \text{ GeV}/c$
 - $\text{prob}(\chi^2)[B^0] > 0.001$
- $B^0 \rightarrow J/\psi K_s^0$
 - $p_T(K_s^0) > 1.5 \text{ GeV}/c$
 - $p_T(B^0) > 4.0 \text{ GeV}/c$
 - $L_{xy}(K_s^0) > 0.1 \text{ cm}$
 - $|L_{xy}/\sigma_{xy}|(K_s^0) > 6$
 - $\text{prob}(\chi^2)[B^0] > 0.0001$
- $\Lambda_b^0 \rightarrow J/\psi \Lambda^0$
 - $p_T(\Lambda^0) > 2.6 \text{ GeV}/c$
 - $p_T(\Lambda_b^0) > 4.0 \text{ GeV}/c$
 - $L_{xy}(\Lambda^0) > 0.1 \text{ cm}$
 - $|L_{xy}/\sigma_{xy}|(\Lambda^0) > 4$
 - $\text{prob}(\chi^2)[\Lambda_b^0] > 0.0001$

The reconstructed B invariant mass distributions can be seen in the section III. For B^+ and B^0 modes, only candidates with a reconstructed B mass between 5.17 and 5.39 GeV/c^2 are used for the lifetime measurements. For the Λ_b^0 mode the mass range is set to 5.43 - 5.83 GeV/c^2 . The quantity \mathbf{V} in equation 2 is estimated from the the transverse decay length L_{xy} of the J/ψ with respect to the beam spot. The quantity \vec{p}_T is estimated from refitted tracks constrained by the full kinematic fit to the b hadron. The proper decay time uncertainty σ_{ct} , includes uncertainties in both the beamspot and the J/ψ vertex. Uncertainties in transverse momentum are negligible, due to the excellent momentum resolution of the COT. We apply a cut of $\sigma_{ct} < 100 \mu\text{m}$ to insure that events used in lifetime measurement have well-measured proper decay times. The invariant mass distributions for B^+ , $B^0(K^{*0}$ and K_s^0 modes) and Λ_b^0 are shown in the Figs. 4, 5, 6 and 7 (first plot). We find the following yield of signal events (to the closest 10):

- B^+ : 45000 ± 230
- B^0 : 16860 ± 140 (K^{*0} mode)
- B^0 : 12070 ± 120 (K_s^0 mode)
- Λ_b^0 : 1710 ± 50

III. THE LIKELIHOOD, PARAMETRIZATION AND FIT METHOD

A. The Likelihood

To extract the signal yields and b -hadron lifetimes, we perform a simultaneous unbinned maximum likelihood fit to the reconstructed mass m , the reconstructed proper decay time ct , and the reconstructed proper decay time uncertainty σ_{ct} . Candidate-by-candidate mass uncertainties σ_m are also used as input to the fit; their distribution is observed to be indistinguishable between signal and background, and thus they are given a different (and simpler)

treatment than the proper decay time uncertainties σ_{ct} , whose distribution differs markedly for signal events and background events. In this section we develop a description of the likelihood function used in the fit. This likelihood function is a sum of two terms (one for signal and one for background), each term being a product of three probability densities; one for mass, one for proper decay time, and one for proper decay time uncertainty:

$$\begin{aligned} \mathcal{L}(m, ct, \sigma_{ct} | \sigma_m) &= f_s \cdot P_m^s(m | \sigma_m) \cdot T_t^s(ct | \sigma_{ct}) \cdot S_t^s(\sigma_{ct}) \\ &+ (1 - f_s) \cdot P_m^b(m) \cdot T_t^b(ct | \sigma_{ct}) \cdot S_t^b(\sigma_{ct}). \end{aligned} \quad (4)$$

Here, $P_m^s(m | \sigma_m)$, $T_t^s(ct | \sigma_{ct})$, and $S_t^s(\sigma_{ct})$ are normalized probability densities in mass m , proper decay time ct , and proper decay time uncertainty σ_{ct} , for the signal; $P_m^b(m)$, $T_t^b(ct | \sigma_{ct})$, and $S_t^b(\sigma_{ct})$ are the same probability distributions for the background, and f_s is the fraction of signal events. In the following we describe each component of the likelihood function in more detail.

B. The mass distribution model

We model the mass distribution of signal events $P_m^s(m | \sigma_m)$ using the sum of two Gaussians centered on the b hadron mass m_0 . Each Gaussian has a width determined by candidate-by-candidate mass uncertainties σ_m scaled by a collective scale factor, s_{m1} for the first Gaussian and s_{m2} for the second:

$$\begin{aligned} P_m^s(m | \sigma_m) &\equiv \frac{f_m}{\sqrt{2\pi}s_{m1}\sigma_m} e^{-(m-m_0)^2/2(s_{m1}\sigma_m)^2} + \frac{1-f_m}{\sqrt{2\pi}s_{m2}\sigma_m} e^{-(m-m_0)^2/2(s_{m2}\sigma_m)^2} \\ &\equiv P_m^s(m; m_0, s_{m1}, f_m, s_{m2} | \sigma_m). \end{aligned} \quad (5)$$

A fraction f_m of the total probability is assigned to the first Gaussian and $1 - f_m$ to the second Gaussian. The mass model for background events is a normalized first-order polynomial:

$$\begin{aligned} P_m^b(m) &\equiv [P_0 + P_1 \cdot (m - m_c)] \\ &\equiv P_m^b(m; P_1), \end{aligned} \quad (6)$$

where P_1 is a floating parameter of the fit while P_0 is determined by normalization and m_c is the center of the mass range. In table I we summarize the parameters of the mass model.

Name	Description	Comments
m_0	b hadron mass	Mass, signal
s_{m1}	Mass Uncertainty Scale Factor	Mass, signal
s_{m2}	2nd Mass Uncertainty Scale Factor	Mass, signal
f_m	Relative fraction between the two signal components	Mass, signal
P_1	Background Slope	Mass, background
f_s	Signal Fraction	Mass, Decay time, Decay time uncertainty

TABLE I: Table listing the fit parameters for the mass model

C. The proper decay time uncertainty distribution parameterization

We apply a cut on the proper time uncertainty distribution at $\sigma_{ct}^{max}=100 \mu\text{m}$. We model the proper time uncertainty distributions using a superposition of normalized components, given by:

$$S(\sigma_{ct}; a, b) = \frac{(\sigma_{ct})^a e^{-(\sigma_{ct})/b}}{b^{a+1} \gamma(a+1, \sigma_{ct}^{max}/b)}. \quad (7)$$

Here the function

$$\gamma(a+1, \sigma_{ct}^{max}/b) \equiv \int_0^{\sigma_{ct}^{max}/b} u^a e^{-u} du = P(a+1, \sigma_{ct}^{max}/b) \cdot \Gamma(a+1),$$

where $\Gamma(a)$ is a normal gamma function and $P(a, x)$ is an incomplete gamma function. We use two such components to model the signal, and three to model the background, except in the case of the Λ_b^0 , where the fraction of one of third background component floats to zero in the fit, and is therefore removed. A summary of the parameters that describe the lifetime uncertainty distribution is given in Table II.

Name	Description	Comments
a_1^s	a-parameter, signal, first component	PDL uncertainty, signal
b_1^s	b-parameter, signal, first component (cm)	PDL uncertainty, signal
a_2^s	a-parameter, signal, second component	PDL uncertainty, signal
b_2^s	b-parameter, signal, second component (cm)	PDL uncertainty, signal
a_1^b	a-parameter, background, first component	PDL uncertainty, background
b_1^b	b-parameter, background, first component (cm)	PDL uncertainty, background
a_2^b	a-parameter, background, second component	PDL uncertainty, background
b_2^b	b-parameter, background, second component (cm)	PDL uncertainty, background
a_3^b	a-parameter, background, third component	PDL uncertainty, background
b_3^b	b-parameter, background, third component (cm)	PDL uncertainty, background
f_1^s	fraction of signal in first component	PDL uncertainty, signal
f_1^b	fraction of background in first component	PDL uncertainty, background
f_2^b	fraction of remainder (background) second component	PDL uncertainty, background

TABLE II: Table listing the fit parameters for proper time uncertainty model. PDL refers to the proper decay length as defined in Equation(3).

D. The proper decay time distribution parameterization

1. Signal Events

The distribution of proper decay time for ideal signal events is an exponential distribution with characteristic decay constant λ . However, neither the primary nor the secondary vertex, which are used to determine the event proper decay length, are measured with perfect accuracy. Therefore in the observed measurements, the detector resolution smears the measured vertex point from the true vertex point, and the primary vertex in each event fluctuates within the envelope of the beam spot. We model the signal events as a decaying exponential convolved with a description of these resolution effects. Our model for these effects, and how it is determined will be described in the next few subsections.

2. Background Events

Our model for the background consists of (1) prompt J/ψ events, (2) real and fake J/ψ events from heavy flavor. The prompt events are taken to have transverse decay length errors that scale in the same way as in signal events, while other background events are not assumed to scale that way, since the vertices may be fake. The prompt component constrains therefore the detector resolution, while the remaining events are modeled by a sum of functions described by

$$T(ct; \bar{\tau}, s_t | \sigma_{ct}) = \int \frac{1}{\bar{\tau}} e^{-t/\bar{\tau}} \cdot \frac{1}{\sqrt{2\pi} \cdot s_t \cdot \sigma_{ct}} e^{-(ct-c\tau)^2/2(s_t\sigma_{ct})^2} d(ct), \quad (8)$$

the parameters $\bar{\tau}$ and s_t being the effective lifetime and proper time uncertainty scale factor. In this expression the parameter $\bar{\tau}$ may be positive, indicating a positive exponential, or negative, indicating a negative exponential. We use 2 positive exponential components and one negative exponential component. For the all decay modes we use the following parametrization:

$$\begin{aligned} T_t^b(ct; s_t, f_g, f_{++}, f_-, \lambda_+, \lambda_{++}, \lambda_- | \sigma_{ct}) = & f_g \cdot \mathcal{R} \\ & + (1 - f_g) \cdot (f_{++} \cdot T(ct; \lambda_{++} s_t | \sigma_{ct}) \\ & + (1 - f_{++}) \cdot [f_- \cdot T(ct; -\lambda_-, s_t | \sigma_{ct}) \\ & + (1 - f_-) \cdot T(ct; \lambda_+, s_t | \sigma_{ct})], \end{aligned} \quad (9)$$

where \mathcal{R} is the resolution function and f_g is the prompt fraction of the background; of the remainder f_{++} is the fraction which is attributed to a positive exponentially decreasing component described by a lifetime λ_{++} ; of the remainder f_- is the fraction associated with a negative exponentially decreasing background with a lifetime of λ_- ; and the remainder is associated with an exponentially decreasing background with lifetime λ_+ . The scale factor st_1 is used for all components.

3. The Resolution model and determining its parameters

We base our resolution model on a superposition of three Gaussians; the restriction to models symmetric about $t = 0$ is motivated by simulation, while the shape and size of the resolution, and the number of components, is determined from data. The width of each component is determined by candidate-by-candidate proper decay uncertainties σ_{ct} , scaled by a collective scale factor, s_1 for the first Gaussian, s_2 for the second, and s_3 for the third. If $G(m, w)$ represents a Gaussian of width w and mass m , then the resolution model is written as

$$\mathcal{R} = f_1 \times G(0, s_1\sigma_{ct}) + f_2 \times G(0, s_2\sigma_{ct}) + f_3 \times G(0, s_3\sigma_{ct}), \quad (10)$$

where $f_1 + f_2 + f_3 = 1$. Five floating components are required to fit this (two fractions and 3 scale factors).

To extract the parameters that determine the shape of the resolution we use the background sample, obtained from mass sideband regions to simultaneously fit the resolution shape and the other background proper decay time parameters. The sideband regions for the charged and neutral meson are defined by those where the mass of the candidate, M_B lies between $5.17 < M_B < 5.22 \text{ GeV}/c^2$ or $5.33 < M_B < 5.39 \text{ GeV}/c^2$. For the Λ_b^0 the sideband region is defined as $5.48 < M_B < 5.57 \text{ GeV}/c^2$ or $5.67 < M_B < 5.76 \text{ GeV}/c^2$. We observe that the resolution model is different for different values of σ_{ct} . Therefore, we bin the sideband into 3 bins of σ_{ct} : 0-30 μm , 30-40 μm and 40-100 μm . This splits the data into roughly 3 equal parts. We determine the components of the resolution model separately in each bin of σ_{ct} .

4. The Lifetime fit

Using the likelihood function described in this section, we carry out an unbinned maximum likelihood fit to the data in each of the five channels. The parameters described in this section, in addition to the physics parameter τ_B , are allowed to float; we fix, however, the parameters that determine the resolution shape to the values from the sideband only fit; this procedure has a negligible effect on lifetime estimation, but is helpful in allowing the CPU-intensive fits to run many thousands of times in the evaluation of systematic uncertainties (see section IV). The full set of parameters used in the fit are described in the Tables I, II and III.

Name	Description	Comments
τ_B	b hadron lifetime	Proper decay time, signal
λ_+	Effective background lifetime, pos. component 1	Proper decay time, background
λ_{++}	Effective background lifetime, pos. component 2	Proper decay time, background
λ_-	Effective background lifetime, neg. component	Proper decay time, background
f_p	Fraction of background which is prompt	Proper decay time, background
f_-	Fraction of remainder which is in neg. tail	Proper decay time, background
f_{++}	Fraction of remainder which is in component 2	Proper decay time, background
st_1	Scale factor for the exponential components	Proper decay time, background

TABLE III: Table listing the fit parameters for proper decay time model that are used in the fit to all data.

Various projections of the likelihood function are compared with the data in Fig. 4, 5, 6 and 7. In Fig. 8, 9, 10, and 11, we show the residual and residual significance distributions using the three component resolution model for the signal and sidebands regions.

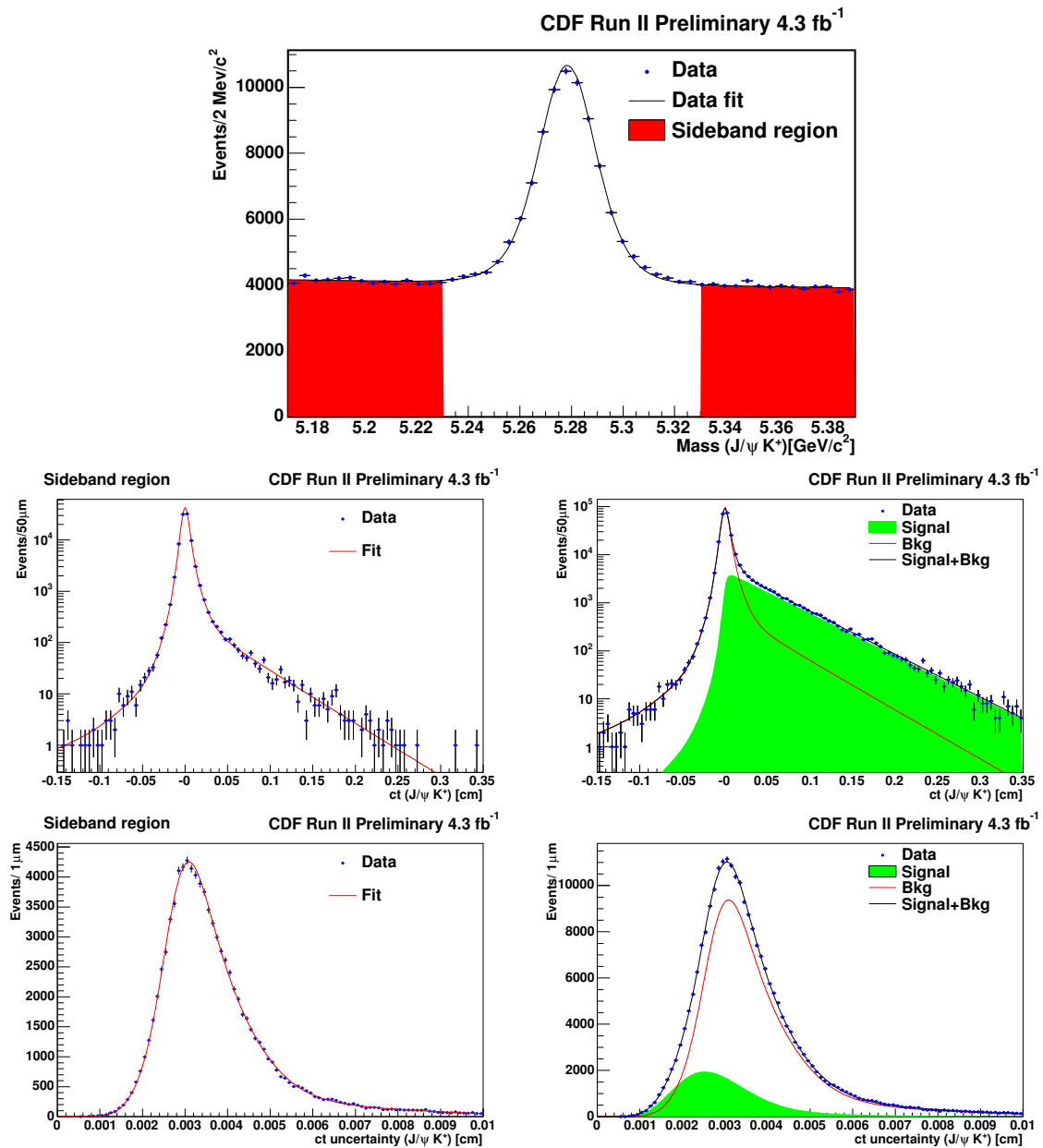


FIG. 4: $B^+ \rightarrow J/\psi K^+$. This figure shows the mass, proper decay length, and proper decay length uncertainty, fit projections. The plots on the left show only the sideband region, the plots on the right show the fit projection over the full mass range used.

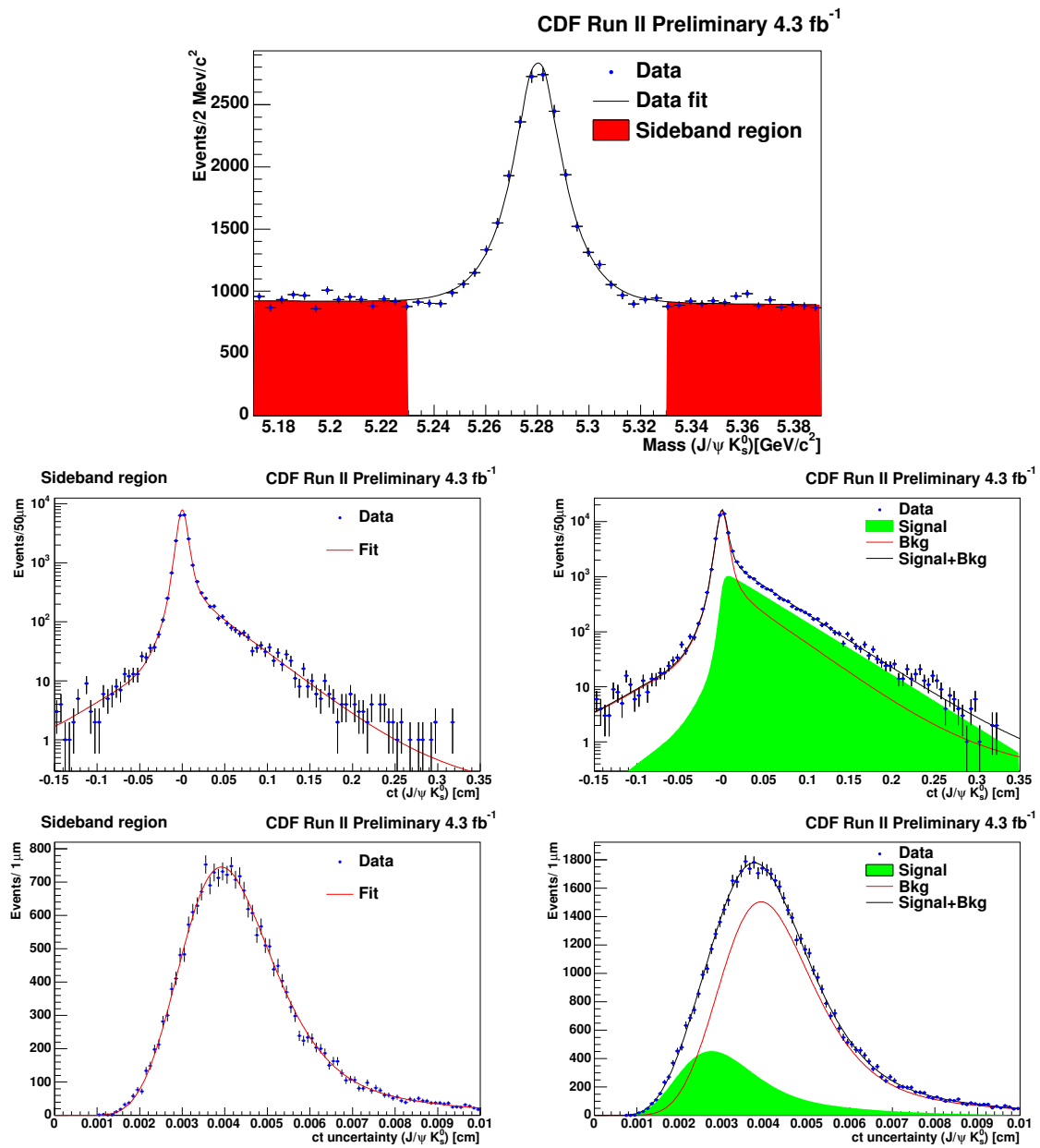


FIG. 6: $B^0 \rightarrow J/\psi K_s^0$. This figure shows the mass, proper decay length, and proper decay length uncertainty, fit projections. The plots on the left show only the sideband region, the plots on the right show the fit projection over the full mass range used.

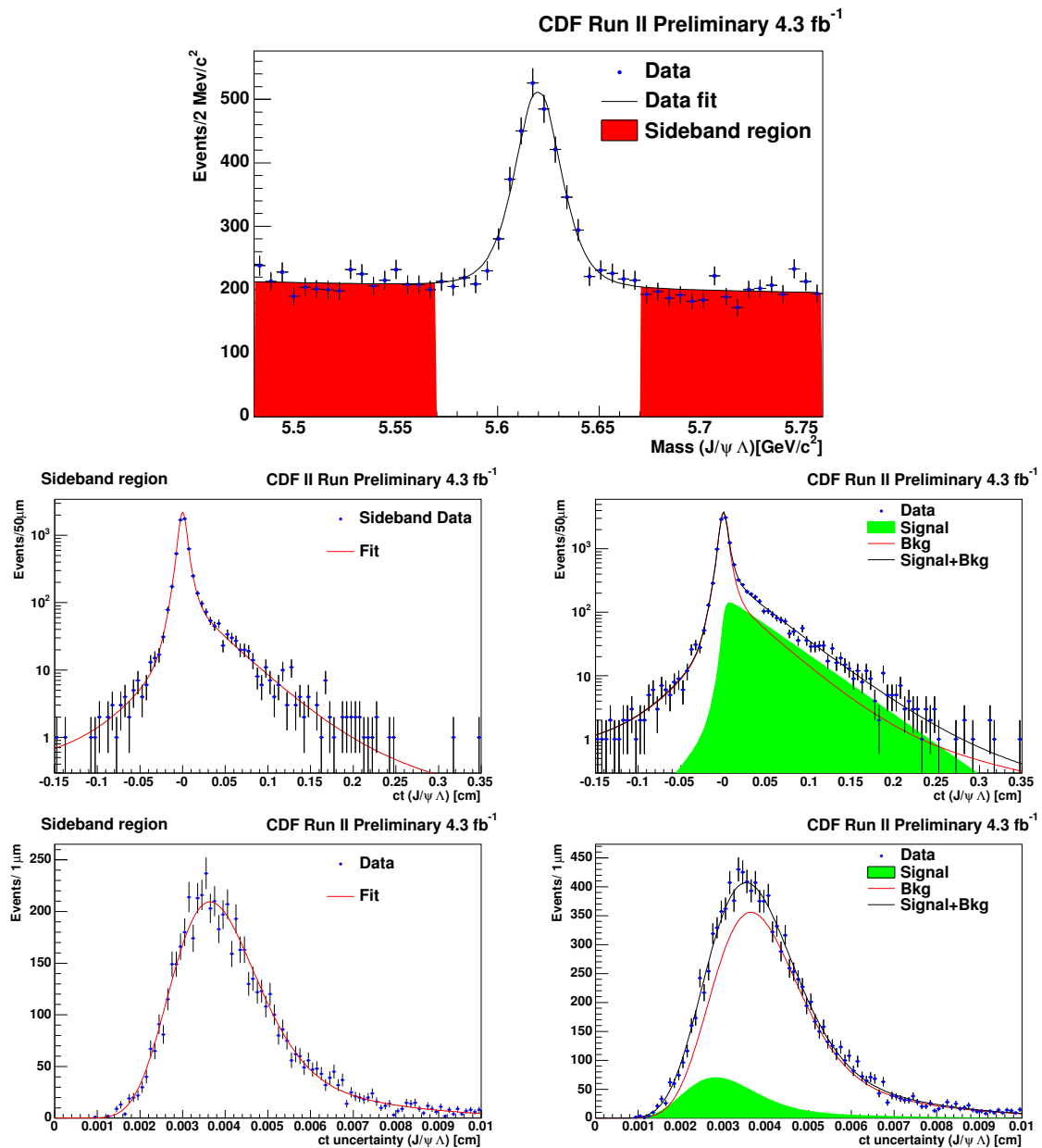


FIG. 7: $\Lambda_b^0 \rightarrow J/\psi \Lambda^0$. This figure shows the mass, proper decay length, and proper decay length uncertainty, fit projections. The plots on the left show only the sideband region, the plots on the right show the fit projection over the full mass range used.

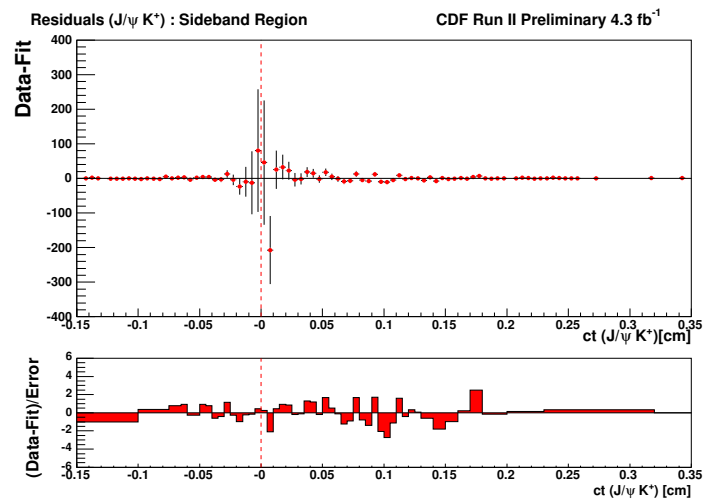
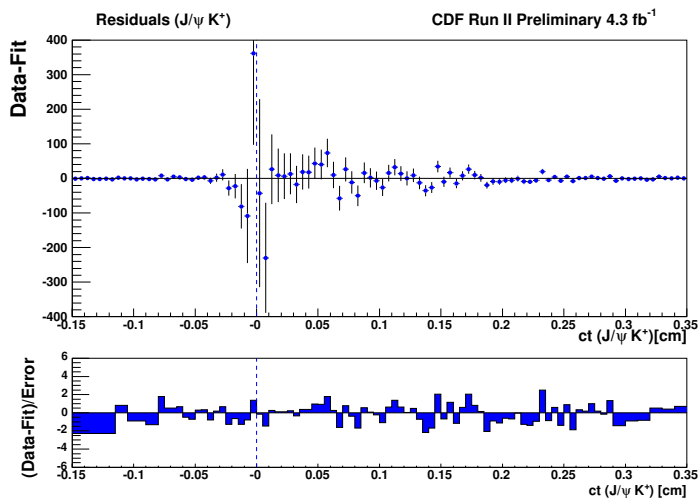


FIG. 8: $B^+ \rightarrow J/\psi K^+$ residual for the lifetime projection. Left(right) plots correspond to the signal (sidebands) region respectively.

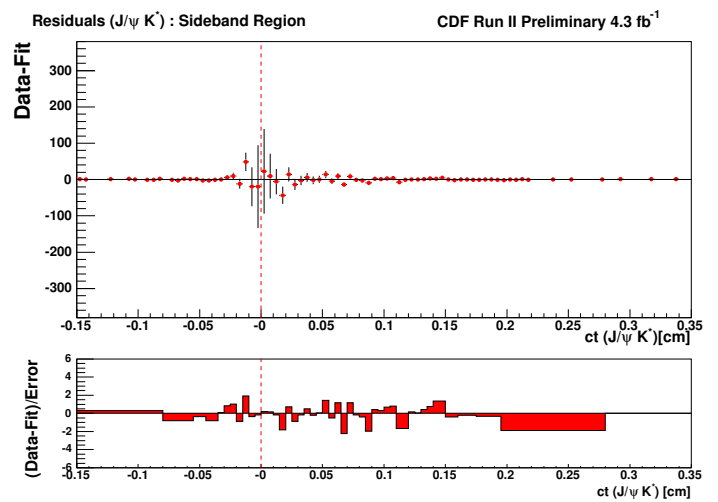
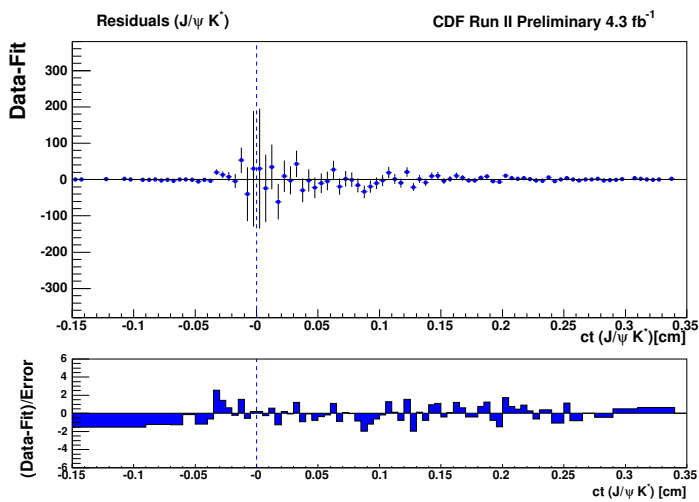


FIG. 9: $B^0 \rightarrow J/\psi K^{*0}$ residual for the lifetime projection. Left(right) plots correspond to the signal (sidebands) region respectively.

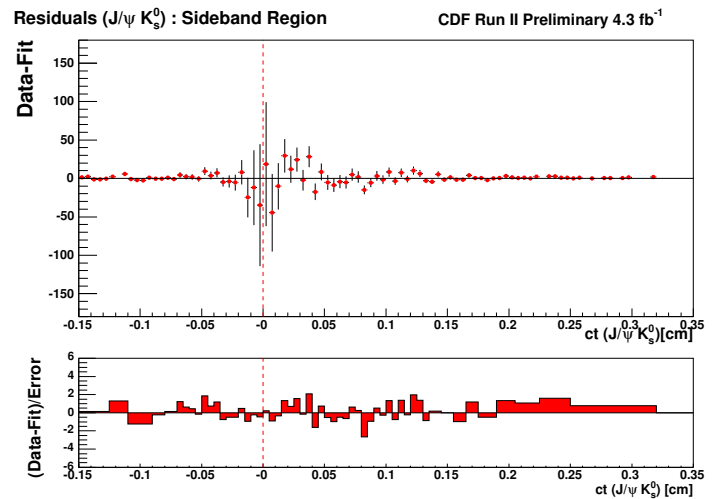
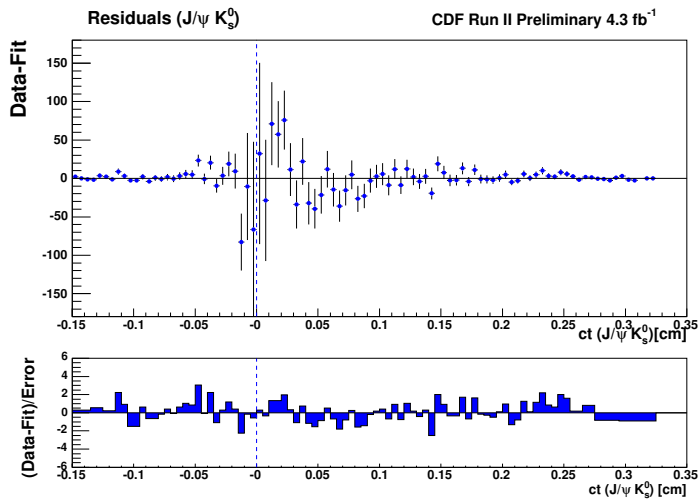


FIG. 10: $B^0 \rightarrow J/\psi K_s^0$ residual for the lifetime projection. Left(right) plots correspond to the signal (sidebands) region respectively.

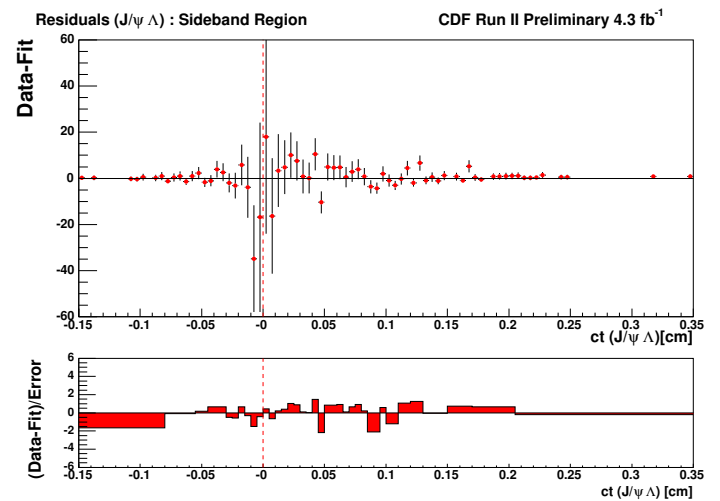
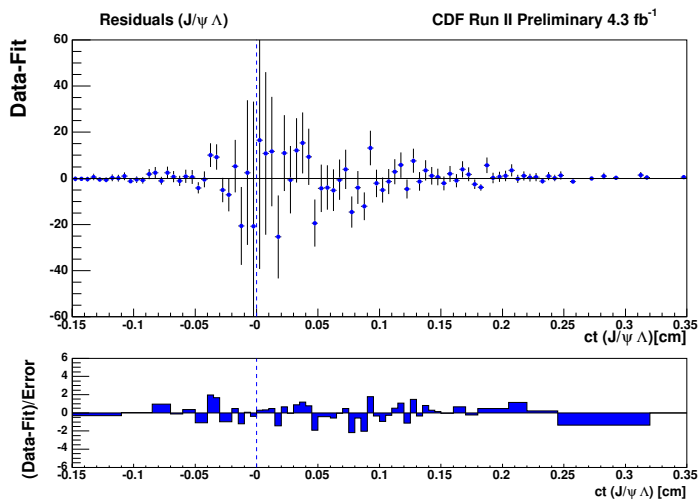


FIG. 11: $\Lambda_b^0 \rightarrow J/\psi \Lambda^0$ residual for the lifetime projection. Left(right) plots correspond to the signal (sidebands) region respectively.

IV. SOURCES OF SYSTEMATIC UNCERTAINTY

We considered correlated and uncorrelated systematic uncertainties in this analysis. By correlated, we mean that the uncertainty affects all of the measured lifetimes in an identical way, and therefore results in negligible uncertainty in the ratio of lifetimes.

The leading source of systematic uncertainty for the lifetime measurements is the silicon detector alignment. This uncertainty is evaluated in full simulation by moving the silicon layer detectors in and out and bowing them in and out by the $50 \mu\text{m}$ uncertainty estimated by the alignment group. This uncertainty will be of similar size and direction for all modes and it is therefore treated as a correlated uncertainty when combining results and calculating ratios.

The XFT trigger assumes that the tracks come from the center of the beam. This may introduce a bias for triggering long-lived decays. The trigger bias from the XFT, while expected to be negligible is assessed and treated as correlated. We tested this by simulating the XFT response in many millions of fully simulated events. No indication of any bias was found but a small uncertainty is assigned due to the limited statistical precision of the evaluation method.

Another systematic uncertainty that is treated as correlated is the correlation between reconstructed mass and proper decay length uncertainty which has been ignored in the derivation of the likelihood. This was, however, found to have a negligible effect on lifetime measurement.

Other systematic uncertainties were determined using a simplified Monte Carlo method where many pseudo-experiments are generated according to an alternate probability density function (PDF). The parameters for the alternate PDF were derived from data. These samples are then fitted with the default PDF and the mean shifts observed on many samples is taken as the systematic uncertainty.

Historically one of the leading sources of uncertainty in a lifetime analysis has been the uncertainty in the resolution modeling. This analysis has attempted to minimize such sources of uncertainty by a careful modeling of the detector resolution; the remaining sources of uncertainty due to the determination of the resolution model have been multiply tested.

Since the resolution is determined from the prompt events, and the shape of those events is sensitive to the modeling of long-lived (positive and negative) background, uncertainties in the background modeling can affect the lifetime through the resolution model. We account for that uncertainty by including an extra long-lived component in the background model. This alternate description produces a substantial change in the fraction of prompt events (approximately 7%) and has a small but non-negligible effect on the lifetime. Other variations that we tried were generally not consistent with the data and were ruled out.

Since the proper time scale factors s_1 , s_2 , and s_3 are each determined in three bins of proper time uncertainty σ_{ct} , we consider the binning as an additional source of uncertainty, which we evaluate by using five bins in σ_{ct} and quantifying the effect using simplified Monte Carlo.

Other sources of uncertainty relate to the parameterization of the distributions of mass m , proper decay length uncertainty σ_{ct} , and proper decay length ct distributions (the latter applying essentially in the modeling of background). To evaluate uncertainties in the mass model, alternate parameterizations, including a 2^{nd} order polynomial for background and a single Gaussian to describe signal events, were considered. The background decay length parameterisation uncertainty is determined by introducing an extra long lived component into the background model; additionally, we introduced an extra Gaussian component that was not part of the resolution. We varied the σ_{ct} distribution by reducing the number of components in signal and background. On its own, this change gave a poor fit to the data, but simultaneously shifting the distribution by replacing σ_{ct}^a with $(\sigma_{ct} - c)^a$ (c a floating constant) gave a reasonable alternate parameterisation and a small contribution to the overall systematic uncertainty. We also considered the effect of ignoring any differences between signal and background mass uncertainties by using distributions determined from data to generate the values of the mass uncertainty in the simplified Monte Carlo, again we obtain a small contribution to the overall systematic uncertainty.

Two further sources of uncertainty that are specific to particular decays channels are the presence of the Cabibbo suppressed channel $B^+ \rightarrow J/\psi\pi^+$ in the charged B decays and the effect of a swapping the kaon and pion hypotheses in K^* reconstruction. These were evaluated using the simplified Monte Carlo and make a small contribution to the overall systematic uncertainty.

The results of the systematic studies are summarized in Table IV where each individual contribution to the lifetime and the ratio is given along with the total systematic uncertainty assigned. We define the ratios as $R_+ = \frac{\tau(B^+)}{\tau(B^0)}$ and $R_\Lambda = \frac{\tau(\Lambda_b)}{\tau(B^0)}$. While the overall systematic uncertainties remain small, the uncertainty on the extracted lifetime values is dominated by the alignment uncertainty (resolution effects in the case of the Λ_b^0). For lifetime ratios, the total uncertainty has larger contributions from systematic uncertainties due to resolution and mass models.

	$J/\psi K^+$	$J/\psi K^{*0}$	$J/\psi K_s^0$	$J/\psi \Lambda^0$	R_+	R_Λ
Alignment	2.0 (μm)	-	-			
Resolution ($\sigma_{c\tau}$ binning)	0.61 (μm)	0.17 (μm)	0.76 (μm)	1.00 (μm)	0.0016	0.0023
Resolution (alternate Bkg model)	0.42 (μm)	1.05 (μm)	0.47 (μm)	2.48 (μm)	0.0018	0.0057
Background model (extra gaussian)	0.30 (μm)	0.14 (μm)	0.30 (μm)	1.32 (μm)	0.0007	0.0030
Background model (extra lifetime component)	0.06 (μm)	0.69 (μm)	1.20 (μm)	0.36 (μm)	0.0015	0.0016
Mass model (2^{nd} order pol. for bkg.)	0.30(μm)	0.30(μm)	0.30(μm)	0.30(μm)	0.0003	0.0004
Mass model (signal model)	0.80(μm)	0.80(μm)	0.80(μm)	0.80(μm)	0.0020	0.0017
PDL uncertainty	0.50 (μm)	0.50 (μm)	0.50 (μm)	1.30 (μm)	0.0010	0.0029
Mass uncertainty	0.90 (μm)	0.0020	0.0012			
Cabibbo suppressed mode in B^+	0.20 (μm)	-	-	-	0.0004	-
Swapped track assignment in B^0	-	0.20 (μm)	-	-	-	-
Possible Trigger Bias	0.50 (μm)	-	-			
$\sigma_{c\tau}$ - m correlation	0.20 (μm)	-	-			
Total -	± 2.6 (μm)	± 2.8 (μm)	± 2.9 (μm)	± 4.1 (μm)	0.0043	0.0079

TABLE IV: Summary of systematic uncertainties applied to the lifetime measurements. In this table, some errors are applied uniformly to all of the channels, where appropriate, where no difference between modes is expected. PDL refers to proper decay length. In this table we use the symbols $R_+ = \tau_{B^+}/\tau_{B^0}$ and $R_\Lambda = \tau_{\Lambda_b}/\tau_{B^0}$.

V. RESULTS AND CONCLUSION

We have measured the lifetimes of decays of B^+ and B^0 mesons to a J/ψ and a kaon, and Λ_b^0 baryon to a J/ψ and a Λ^0 . The resulting b hadron lifetimes are:

$$\begin{aligned}
c\tau(B^+ \rightarrow J/\psi K^+) &= 491.4 \pm 2.6 (stat.) \pm 2.6 (syst.) \mu\text{m} \\
c\tau(B^0 \rightarrow J/\psi K^{*0}) &= 450.4 \pm 4.0 (stat.) \pm 2.8 (syst.) \mu\text{m} \\
c\tau(B^0 \rightarrow J/\psi K_s^0) &= 453.6 \pm 4.8 (stat.) \pm 2.9 (syst.) \mu\text{m} \\
c\tau(\Lambda_b^0 \rightarrow J/\psi \Lambda^0) &= 460.8 \pm 13.4 (stat.) \pm 4.1 (syst.) \mu\text{m}
\end{aligned}$$

We combine the two B^0 measurements into a single lifetime measurement performing its weighted mean. The result is:

$$c\tau_{B^0} = 451.7 \pm 3.0(stat.) \pm 2.5(syst.)\mu\text{m} \quad (11)$$

The corresponding value for the lifetimes in picoseconds is :

$$\begin{aligned}
\tau_{B^+} &= 1.639 \pm 0.009 (stat.) \pm 0.009 (syst.) \text{ ps} \\
\tau_{B^0} &= 1.507 \pm 0.010 (stat.) \pm 0.008 (syst.) \text{ ps} \\
\tau_{\Lambda_b^0} &= 1.537 \pm 0.045 (stat.) \pm 0.014 (syst.) \text{ ps}
\end{aligned}$$

Finally, we calculate the ratio of lifetimes.

$$\begin{aligned}
\tau_{B^+}/\tau_{B^0} &= 1.088 \pm 0.009 (stat.) \pm 0.004 (syst.) \\
\tau_{\Lambda_b^0}/\tau_{B^0} &= 1.020 \pm 0.030 (stat.) \pm 0.008 (syst.)
\end{aligned}$$

Figs.12 to 15 show the comparison of this measurement with other recent measurements and PDG values. The CDF measurements PRL 94 101803 (Acosta(05)) and PRL 98 122001 (CDF II $\Lambda_b^0 \rightarrow J/\psi \Lambda$, 1 fb^{-1}) contain data that have been used in these measurements.

$\tau(B^+)$ measurements

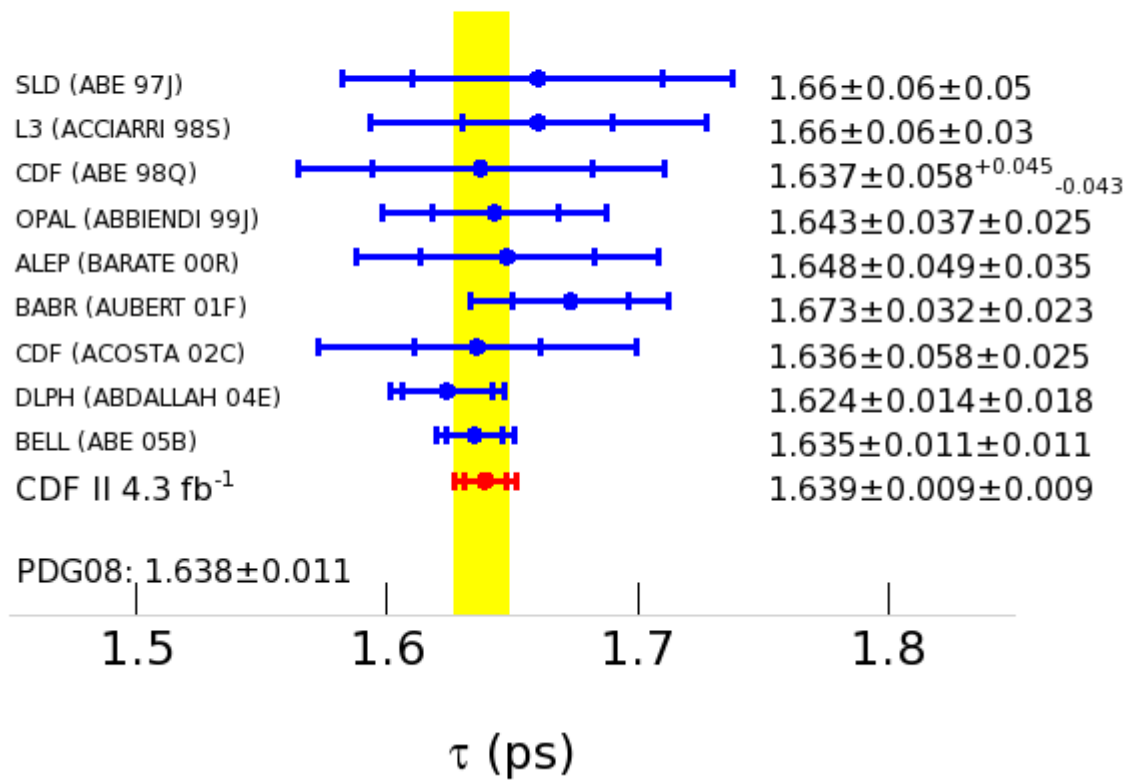


FIG. 12: A comparison of the B^+ lifetime with other recent measurements.

$\tau(B^0)$ measurements

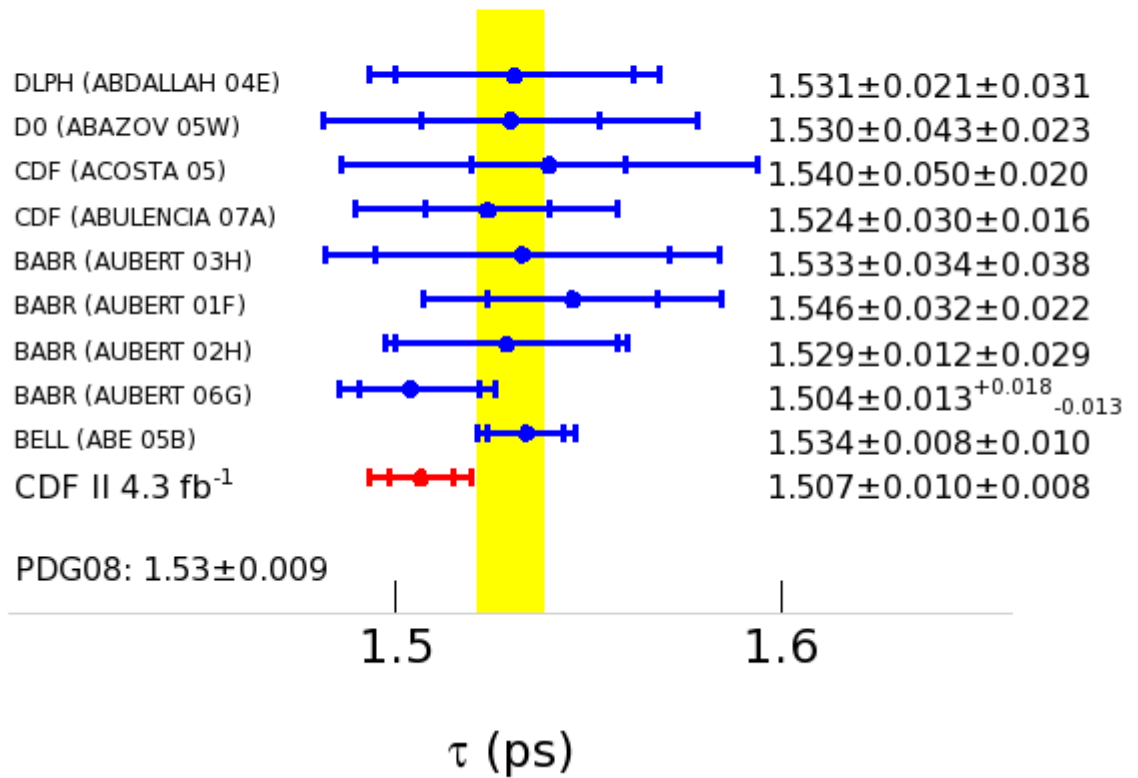


FIG. 13: A comparison of the B^0 lifetime with other recent measurements.

$\tau(B^+)/\tau(B^0)$ measurements

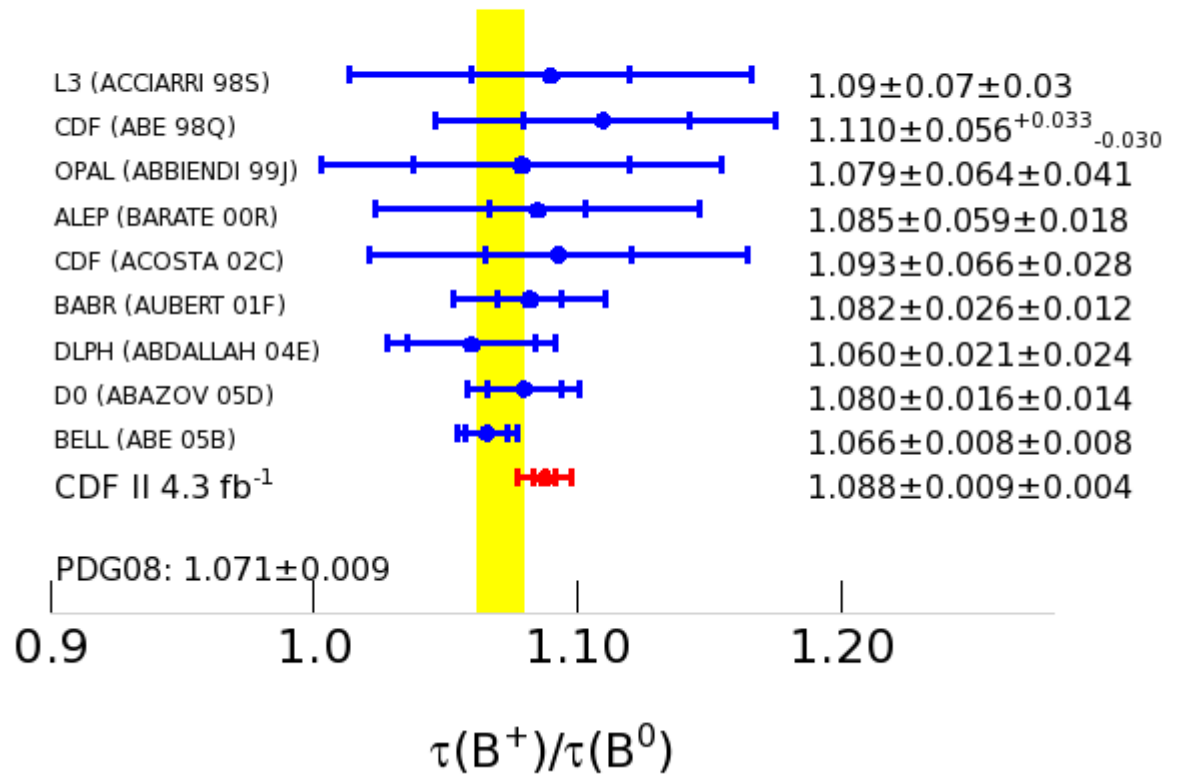


FIG. 14: A comparison of the ratio τ_+/τ_- with other recent measurements.

$\tau(\Lambda_b^0)$ measurements

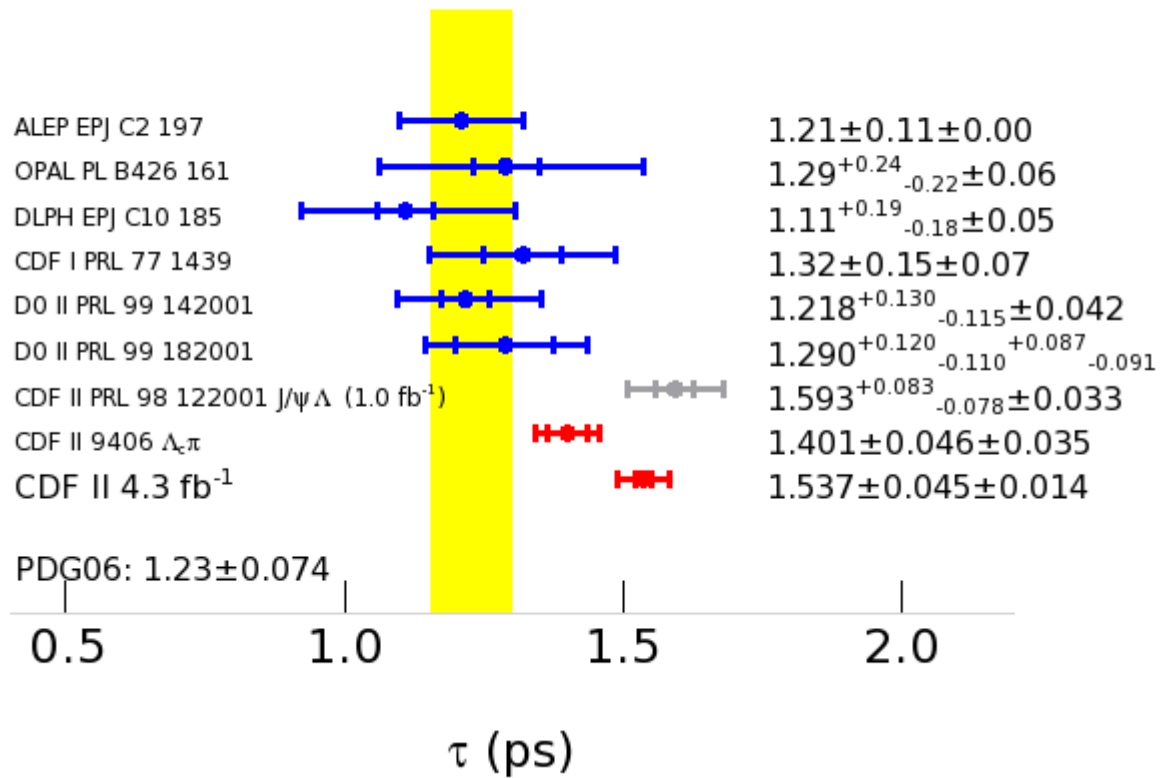


FIG. 15: A comparison of the Λ_b^0 lifetime with other recent measurements. For this comparison we choose the world average value from PDG06, which contains neither the previous CDF measurement (in gray) nor the recent CDF measurement based on $\Lambda_b^0 \rightarrow \Lambda_c^+ \pi^-$.

Acknowledgments

We thank the Fermilab staff and the technical staffs of the participating institutions for their vital contributions. This work was supported by the U.S. Department of Energy and National Science Foundation; the Italian Istituto Nazionale di Fisica Nucleare; the Ministry of Education, Culture, Sports, Science and Technology of Japan; the Natural Sciences and Engineering Research Council of Canada; the National Science Council of the Republic of China; the Swiss National Science Foundation; the A.P. Sloan Foundation; the Bundesministerium für Bildung und Forschung, Germany; the World Class University Program, the National Research Foundation of Korea; the Science and Technology Facilities Council and the Royal Society, UK; the Institut National de Physique Nucleaire et Physique des Particules/CNRS; the Russian Foundation for Basic Research; the Ministerio de Ciencia e Innovación, and Programa Consolider-Ingenio 2010, Spain; the Slovak R&D Agency; and the Academy of Finland.

-
- [1] C. Amsler *et al.*, (Particle Data Group) Physics Letters **B667** 1 (2008), and 2009 partial update for the 2010 edition.
- [2] C Tarantino Eur. Phys. J. **C33**, S895 (2004), hep-ph/0310241; F. Gabbiani, A. Onishchenko, and A. Petrov Phys. Rev. D68, 114006, 2003.
- [3] F. Gabbiani, A. Onishchenko and A. Petrov, Phys. Rev. **D70** 094031
- [4] I.I. Bigi *et al.*, in *B Decays*, 2nd ed., S. Stone (ed.), World Scientific, Singapore, 1994.
- [5] I. Bigi, private communication.
- [6] The CDF Collaboration, “Measurement of Exclusive B Lifetimes in the modes $B^+ \rightarrow J/\psi K^+$, $B^0 \rightarrow J/\psi K^{*0}$, $B^0 \rightarrow J/\psi K_s^0$, $B_s \rightarrow J/\psi \phi$ and $\Lambda_b \rightarrow J/\psi \Lambda$ ”, <http://www-cdf.fnal.gov/physics/new/bottom/061130.blessed-bh-lifetime.v2>
- [7] <http://arxiv.org/abs/0912.3566>
- [8] K. Abe *et al.* (Belle Collaboration) , Phys. Rev. **D71** 072003 (2005)
- [9] A selection of recent comparable B^+ , B^0 lifetime and lifetime ratio results from PDG2006 and the world average value. Individual measurements:
 ABE97J PRL 79 590 K. Abe et al. (SLD Collab.)
 ACCIARRI 98S PL B438 417 M. Acciarri et al. (L3 Collab.)
 ABE 98Q PR D58 092002 F. Abe et al. (CDF Collab.)
 ABBIENDI 99J EPJ C12 609 G. Abbiendi et al. (OPAL Collab.)
 BARATE 00R PL B492 275 R. Barate et al. (ALEPH Collab.)
 AUBERT 01F PRL 87 201803 B. Aubert et al. (BaBar Collab.)
 AUBERT 02H PRL 89 011802 B. Aubert et al. (BaBar Collab.) Also PRL 89 169903 (erratum) B. Aubert et al. (BaBar Collab.)
 ACOSTA 02C PR D65 092009 D. Acosta et al. (CDF Collab.)
 AUBERT 03H PR D67 091101R B. Aubert et al. (BaBar Collab.)
 ABDALL 04E EPJ C33 307 J. Abdallah et al. (DELPHI Collab.)
 ACOSTA 05 PRL 94 101803 D. Acosta et al. (CDF Collab.)
 ABE 05B PR D71 072003 K. Abe et al. (BELLE Collab.) Also PR D71 079903 (Erratum) K. Abe et al. (BELLE Collab.)
 ABAZOV 05D 05D PRL 94 182001 V.M. Abazov et al. (D0 Collab.)
 ABAZOV 05W PRL 95 171801 V.M. Abazov et al. (D0 Collab.)
 AUBERT 06G PR D73 012004 B. Aubert et al. (BABAR Collab.)
- [10] A selection of recent comparable Λ_b lifetime measurements from PDG2006 and other sources. Individual measurements are:
 ABE 96M PRL 77 1439 F. Abe et al. (CDF Collab.)
 BARATE 98D EPJ C2 197 R. Barate et al. (ALEPH Collab.)
 ACKER 98G PL B426 161 K. Akerstaff et al. (OPAL Collab.)
 ABREU 99W EPJ C10 185 P. Abreu et al. (DELPHI Collab.)
 ABAZOV 05C PRL 94 102001 V.M. Abazov et al. (D0 Collab.)
 D0-5179-Conf D0 Conference Note 5179 August 18, 2006 (D0 Collab.)
 D0 PRL99 182001 V.M. Abazov *et al.* (D0 Collab) PRL 99 182001
 D0 PRL99 142001 V.M. Abazov *et al.* (D0 Collab) PRL 99 142001
 CDFII 9406 CDF Public Note 9506 [arXiv:0912.3566v2]